

Original article

Asymptotic hydrodynamic homogenization and thermodynamic bounds for upscaling multiphase flow in porous media

Shaheryar T. Hussain¹, Klaus Regenauer-Lieb², Aleksandr Zhuravljov³, Furqan Hussain¹, Sheikh S. Rahman¹ *

¹School of Minerals and Energy Resources Engineering, University of New South Wales, Kensington NSW 2033, Australia

²School of Minerals Energy and Chemical Engineering, Curtin University, Kensington WA 6151, Australia

³Centre of Innovation for Flow through Porous Media, University of Wyoming, Laramie WY 82071, USA

Keywords:

Uncertainty bounds
entropy production
multiphase REV
volume of fluid
pore scale modelling

Cited as:

Hussain, S. T., Regenauer-Lieb, K., Zhuravljov, A., Hussain, F., Rahman, S. S. Asymptotic hydrodynamic homogenization and thermodynamic bounds for upscaling multiphase flow in porous media. *Advances in Geo-Energy Research*, 2023, 9(1): 38-53.
<https://doi.org/10.46690/ager.2023.07.05>

Abstract:

This paper presents a novel technique for upscaling multiphase fluid flow in complex porous materials that combines asymptotic homogenization approach with hydrodynamic and thermodynamic bounds. Computational asymptotic homogenization has been widely utilised in solid mechanics as a method for analysing multiscale expansion and convergence coefficients in heterogeneous systems. Computations are performed over several volumes by increasing the size until convergence of the material parameters under different load scenarios is achieved. It works by simplifying the problem with a homogenization method and is ideally suited for estimating the representative elementary volume of microporous material by expanding algorithms. The validity of the method to include complex multiphase hydrodynamic processes and their interaction with the matrix structure of porous media lacks a sound theoretical foundation. To overcome this problem, a variational thermodynamic approach is used. Upper and lower bounds of entropy production are proposed to provide effective material properties with uncertainties. This allows multiple possibilities to address dynamics via thermodynamically linked processes. This work utilizes volume of fluid approach to model multiphase porous media flow in models based on micro-computerized tomography x-ray data of Bentheimer sandstone and Savonnieres carbonate. It is found that the representative elementary volume sizes obtained by the conventional asymptotic homogenization methods do not satisfy thermodynamic bounds which consistently require larger representative elementary volume sizes. For the Savonnieres carbonate the entropic bounds have not converged fully questioning the reliability of the effective properties obtained from the classical method.

1. Introduction

Multiphase transport phenomena are fundamental to petroleum exploration and production, particularly for enhanced oil recovery, CO₂ sequestration, and analysing fluid-rock interphase behaviour (Dai et al., 2014; Khodadadi et al., 2020). Conventionally, laboratory testing of core scale studies has been the primary method for collecting multiphase data, which are time-consuming and error prone. Multiphase modelling has become an essential tool for overcoming the

limits of laboratory studies (Gharbi and Blunt, 2012; Alpak et al., 2018). However, proper benchmarking with real-world data or published literature is necessary (Hussain et al., 2021). Massive attention has been placed on extending this method to many scales, with digital rock analysis serving as a prominent example (Jiang and Tsuji, 2017; Aliseda and Heindel, 2021; Liao et al., 2022; Pirzada et al., 2023).

In recent years, micro-computerized tomography (micro-CT) imaging has played an important role in characterizing

heterogeneous fluid flow processes that were previously inaccessible using traditional core analysis. This has provided vital insight into the three dimensional microstructures of complicated rock geometries. The method is based on combining a series of two dimensional grayscale images containing noise and artefacts, necessitating additional processing for quality improvement while conserving rock features (Sidorenko et al., 2021). Following the application of Bilateral and Non-Local Mean filters, the stack of 2D images is prepared for segmentation (Diwakar and Kumar, 2018). Segmentation is the process of turning the stack into a binary format using either basic thresholding techniques or sophisticated multi thresholding algorithms (Leu et al., 2014). After segmentation, the 3D binary model is prepared for pore scale simulations using two well-known methods: a pore network modelling approach that transforms the pore geometry into a network of pore bodies and pore throats (Dong and Blunt, 2009; Gharbi and Blunt, 2012; Lanetc et al., 2023), and a direct numerical simulation approach which requires discretization of the pore geometry into meshes (Joekar-Niasar et al., 2012; Alpak et al., 2018; Ramstad et al., 2019; Shapoval et al., 2023).

The required resolution of such a model is defined by the smallest pores, while the minimum size of the model is determined by the rock's representative elementary volume (REV) (Costanza-Robinson et al., 2011). An REV is understood as the length scale over which the effects of local heterogeneities on a particular rock property (such as porosity, absolute/effective permeability, Euler characteristics, capillary number, and capillary pressure etc) remain constant (Bear, 1975). This concept provides a smooth average over the discontinuous nature of the data at the pore scale, which can produce enormous changes in property estimations when the length scale is altered slightly. Therefore, REV's provide a continuum volume at which these fluctuations are averaged out thereby providing a link between the pore scale and continuum scale characteristics of porous media. The only disadvantage of micro-CT is the trade-off between scanning resolution and sample size, which varies with each rock type due to the degree of existing heterogeneity (Bultreys et al., 2015). Therefore, it is essential to determine the optimal-resolution (to identify necessary rock properties such as sub-resolution porosity) and -sample size (also known as REV) for the medium of interest. Carbonates and also sandstones in certain instances (Urakov et al., 2021) are prominent examples of such pore size distributions.

Estimating REV is a broad topic of study ranging from geometrical analysis of rock's tomographic data (Al-Raoush and Papadopoulos, 2010) to fluid flow through porous media (Mostaghimi et al., 2013) to poromechanics (Regenauer-Lieb et al., 2014), but all are working towards the same end goal which is the upscaling of rock properties from micro tomographic data. Mostaghimi et al. (2013) calculated the REV size for the Berea sandstone's porosity and permeability and found that the sample size for the permeability is approximately twice as large as that for the porosity. According to Liu et al. (2018a), tight sandstones exhibit REV's for both porosity and permeability, with the permeability REV being approximately four times larger than the porosity REV. Liu

et al. (2021) also investigated the REV size for a Bingham fluid and found that it was identical for single-phase flow of Newtonian and Bingham fluids. They also calculated REV's for effective permeability and pseudo start-up pressure gradient. In addition, sophisticated statistical approaches provide an REV approximation based on a simple geometric examination of rock attributes. However, the methods are unable to characterize the dynamics of fluid flow and can only confirm the validity of the REV assumption based on geometrical reasoning; notable techniques in this regard include the applications of percolation theory (Liu and Regenauer-Lieb, 2021) and Gray Level Size Zone Matrices (Singh et al., 2020), which provide rapid screening for possible REV ranges.

Regarding thermodynamically coupled processes, a solid theoretical foundation for the determination of REV and uncertainty estimations was presented for the first time by Regenauer-Lieb et al. (2014). Using the upper and lower limits of entropy production caused by the hydromechanically cross-coupled thermodynamic forces and fluxes, the technique identifies a minimal size for the REV. These cross-couplings can be substantial and trigger a rich class of dynamic and quasistatic flow pattern for which a robust linear stability analysis of the crucial dynamic coefficients was found (Regenauer-Lieb et al., 2021a, 2021b). Moreover, the volume of fluid (VOF) method permits consideration of these couplings, and it is anticipated that if the instabilities are resolved by the method, the results will be naturally incorporated into the upper and lower bounds of entropy production for estimation of the dissipative properties. This method has only been evaluated once for estimating the permeability of a deep-sea carbonate in Brazil (a Commonwealth Scientific and Industrial Research Organization owned commercial contract, unpublished) and once for estimating rheological parameters for a constitutive plasticity law (Liu et al., 2018b). A scientific application to multiphase fluid flow is still outstanding.

Conventional approaches for determining a geometric REV may yield conflicting findings for samples with a high degree of heterogeneity or under dynamic situations (such as specific force dominated flow or while flowing multiple fluids to acquire relative permeability). This paper evaluates the findings of a hybrid formulation that computes single and multiphase petrophysical properties using finite volume simulations on a series of models with different mesh sizes and increasing dimensions. It was shown by Liu and Wang (2022), the REV calculated using multiphase finite element (FE)-lattice Boltzmann method (LBM) is twice that of single-phase predictions. Our study extends the research conducted by Liu and Wang (2022) for assessing REV's in multiphase fluid flow. As stated, the authors employed an unconsolidated synthetic spherical grains and did not verify thermodynamic consistency of the coupled phenomena using a technique that is strongly based on interaction between the two phases.

This study aims to circumvent the restriction imposed by the conventional methods to employ fluid flow calculations for evaluation of the REV hypothesis. Computation of absolute permeability for REV estimations are mostly based on either pore networks modelling or direct numerical simulations. These single phase flow simulations are frequently used as

a starting point. This study addresses following limitations of traditional methods:

- 1) Apart from LBM, most studies are restricted to single phase flow and ignore cross-coupling between several phases.
- 2) Earlier methods often considered a simplified geometry which is not sufficiently accurate for validation of lab scale results.
- 3) These earlier methods assume the existence of an REV and in most cases, they do not consider an uncertainty quantification of the obtained dissipative property. In few cases, computational asymptotic homogenization methods are used to obtain uncertainty values of the property (Liu and Regenauer-Lieb, 2021) which delivered results that are fully consistent with theoretical thermodynamic limits.
- 4) The cross-coupling between multiple phases can be significant, leading to new dynamic patterns that change the dynamic properties by orders of magnitude and can lead to erroneous determination of REV for cases where internal fluctuations do not converge on thermodynamic bounds.

So far, the difference between asymptotic homogenization REVs and valid thermodynamic REVs has not been investigated. It remains an open question whether the asymptotic homogenization method can automatically satisfy the thermodynamic constraints for all thermodynamically linked phenomena, such as explicitly considering the interaction between multiple phases. In view of this, our study has two primary objectives:

- 1) To benchmark the approach in a new open-source numerical environment without IP-restrictions.
- 2) To evaluate applicability of the technique to coupled multiphase processes.

2. Methodology

2.1 Overview

Fig. 1 illustrates sequential steps in establishing REV of a given petrophysical property using a constant flux (Neumann) boundary condition to derive one bound of asymptotic homogenization of micro-CT data. The other bound is obtained by using a Dirichlet boundary condition for the same problem. Normally, this procedure is very fast when geometrical data is considered, however, when flow dynamics is incorporated, simulation run times increase exponentially. It starts with data acquisition which is followed by filtering and segmentation. Our simulations employ a direct numerical solver method with OpenFoam, an efficient open-source computational fluid dynamics (CFD) solver. It simulates flow of compressible as well as incompressible single-phase and multiphase fluids. The primary purpose of this study is to solve for isothermal and incompressible fluids using the multiphase solver (InterFoam), which is based on Navier Stokes solution of partial differential equations with volume of fluid approach. OpenFoam also offers fundamental tools for generating grid blocks on the pore space area, which is a prerequisite for

simulation runs. Due to the heterogeneous nature of rock pore space, mesh generation is quite complex; consequently, an in-house technique based on the SnappyHexMesh dictionary of OpenFoam requiring a segmented binary image has been devised for mesh development. To save calculation time, variable mesh enlargement criteria, which can be tuned based on the scenario under consideration, has been implemented. In addition, to record petrophysical characteristics for each documented timestep, the InterFoam solver has been updated to produce output of essential values following each simulation run. These quantities are then used to calculate REV for each scenario.

2.2 VOF approach

The VOF technique represents a saturation-based interface capture approach designed for the simulation of two-phase incompressible flows, as established in various studies (Aniszewski et al., 2014; Pavuluri et al., 2018; Karnakov et al., 2020). The underlying equations inherent to this approach, which have been exhaustively examined and are currently deemed conventional, are presented subsequently. For a rigorous analytical exploration of these equations, the authors advise consulting the afore-mentioned reference materials. Analogous to numerous other CFD methodologies, it is predicated upon the conventional form of the continuity equation, albeit, it accommodates two-phase flows:

$$\frac{\partial \rho}{\partial t} + \vec{\nabla} \cdot \rho \vec{v} = 0 \quad (1)$$

where \vec{v} represents velocity and t represents time, the average density, ρ is given by:

$$\rho = \alpha_0 \rho_0 + \alpha_1 \rho_1 \quad (2)$$

where α represents phase saturation and subscripts 0 and 1 represent each phase. Phase saturation conforms to the continuity concept as described below:

$$\alpha_0 + \alpha_1 = 1 \quad (3)$$

The governing equation for saturation, which results from Eqs. (1) and (2), described just for phase 0:

$$\frac{\partial \alpha_0}{\partial t} + \vec{\nabla} \cdot \alpha_0 \vec{v} + \lambda \vec{\nabla} \cdot \alpha_0 (1 - \alpha_0) \max |\vec{v}| \vec{n} = 0 \quad (4)$$

where the third term is responsible for numerical interface compression and λ is its parameter, $\max |\vec{v}|$ is the maximum magnitude of velocity and \vec{n} is the interface normal vector with respect to phase 0 (Rusche, 2003). The robustness of this interphase compression approach is provided by Eq. (3). In the context of this research, the interface compression parameter, denoted as λ , is considered with an assigned value of 1. This value has been found to be conducive for most VOF instances, guaranteeing the preservation of interface integrity (Deshpande et al., 2012). In addition, the momentum conservation equation accounts for capillarity and connects density, velocity, and saturation with pressure (Hirt and Nichols, 1981):

$$\frac{\partial \rho \vec{v}}{\partial t} + \vec{\nabla} \cdot \rho \vec{v} \vec{v} = -\vec{\nabla} p + \vec{\nabla} \cdot \mu \vec{\nabla} \vec{v} + \gamma \vec{\nabla} \cdot \vec{n} \vec{\nabla} \alpha_0 \quad (5)$$

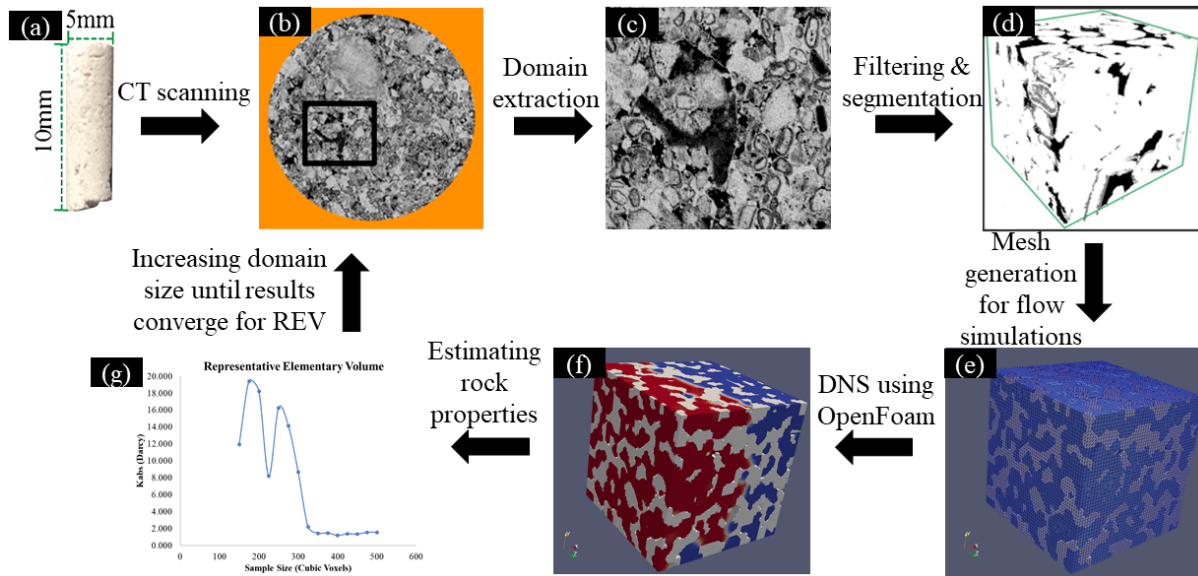


Fig. 1. Flow diagram for pore-scale REV estimation. (a) Extraction of core plug according to the desired resolution, (b) performing micro-CT imaging on the extracted core plug, (c) utilizing custom PythonTM scripts to extract the domain of interest, (d) applying image processing techniques using AvizoTM to isolate the pore space and solid components, (e) discretizing the domain through the SnappyHexMesh utility of OpenFoam, (f) conducting single and multiphase flow simulations using the InterFoam solver, (g) estimating the petrophysical properties of the extracted domain. These steps are iteratively repeated from step (b) until convergence of the petrophysical property is achieved.

where p is pressure and γ is interfacial tension, while average viscosity μ is calculated as below:

$$\mu = a_0\mu_0 + a_1\mu_1 \quad (6)$$

Corresponding boundary conditions must be enforced for the partial differential Eqs. (1), (4) and (5) described above. These can be Neumann or Dirichlet types of boundary conditions regarding saturation a_0 , velocity \vec{v} and pressure p . However, types and values of velocity and pressure boundary conditions should be consistent.

2.3 Simulator and image processing

Considering arbitrary cases, this VOF system of partial differential equations can be solved only numerically. The robust numerical algorithms include pressure-implicit with splitting of operators, semi-implicit method for pressure-linked equations or their combination (Patankar, 2018). These approaches are implemented in the open-source project “OpenFoam”, which is based on the finite volume method (Moukalled et al., 2016) and includes various pre-validated solvers, as well as collections of CFD and auxiliary C++ libraries (Green-shields, 2022).

For this study, the conventional VOF solver “InterFoam” from “OpenFoam” is employed (Deshpande et al., 2012). Moreover, additional functionality for post processing was implemented using “OpenFoam” C++ libraries: calculating volume weighted, cumulative grid-block and boundary flow parameters along with outputting them to convenient JSON files.

For this paper, segmented data was acquired from Bultreys

et al. (2015) and Singh et al. (2020) which are available online at [digital rock portal](#). For Bentheimer sandstone, micro-CT scans were conducted at Tyree X-ray micro-CT facility at University of New South Wales, Sydney, Australia. The facility has a GE Phoenix Nanofocus X-Ray Tube with a diamond window and a high-quality flatbed detector ($3,072 \times 3,072$ pixels, 3.75 fps readout rate) which was designed to allow easy access and the ability to integrate complex flow experiments with the [imaging system](#).

Segmentation was performed using AvizoTM 9.0’s watershed algorithm which is accurate in segmenting surface features to minimize operator bias introduced by arbitrary thresholding grey scale values of pores and solids (Leu et al., 2014). Segmented images were then cropped using custom PythonTM algorithms based on numPy library which allows isotropic increments in domain size of 25^3 voxels (for single phase simulations) and 50^3 voxels (for multiphase simulations) stepped up until REV sizes have been achieved. The size difference between single and multiphase samples has allowed optimization of the simulation runtimes for each scenario. Flow simulations and image processing were carried out on AMD RyzenTM ThreadripperTM PRO 5975WX supported by NVIDIA’s GeForce RTX 3090 GPU and 128 GB of RAM.

2.4 Rock configurations

For two rock configurations, Bentheimer sandstone and Savonnieres carbonate, the asymptotic homogenization technique using constant pressure and velocity constraints was chosen to define hydrodynamic and thermodynamic REV’s for single and multi-phase simulation runs. These rocks were selected based on the variety in their geometrical characteristics.

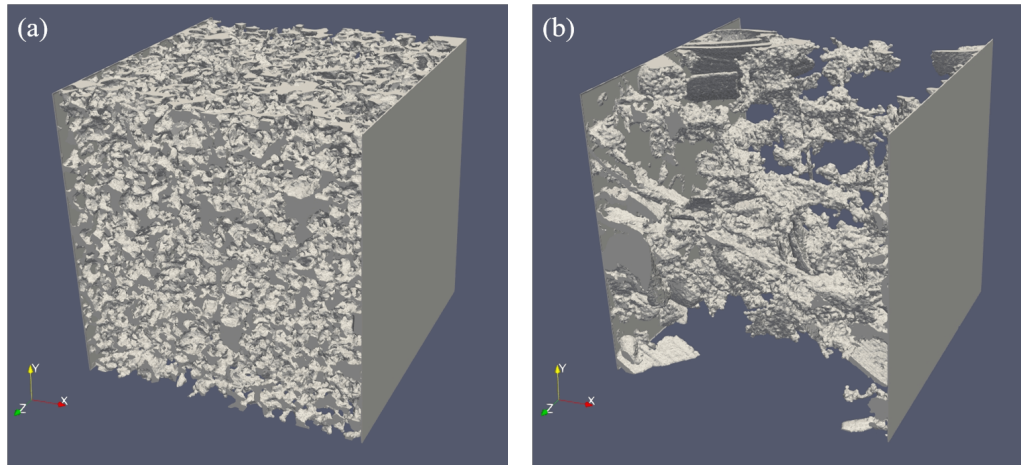


Fig. 2. Pore space representation of (a) Bentheimer sandstone at 600^3 voxels (3.24 mm^3) and (b) Savonnieres carbonate at 1000^3 voxels (3.8 mm^3).

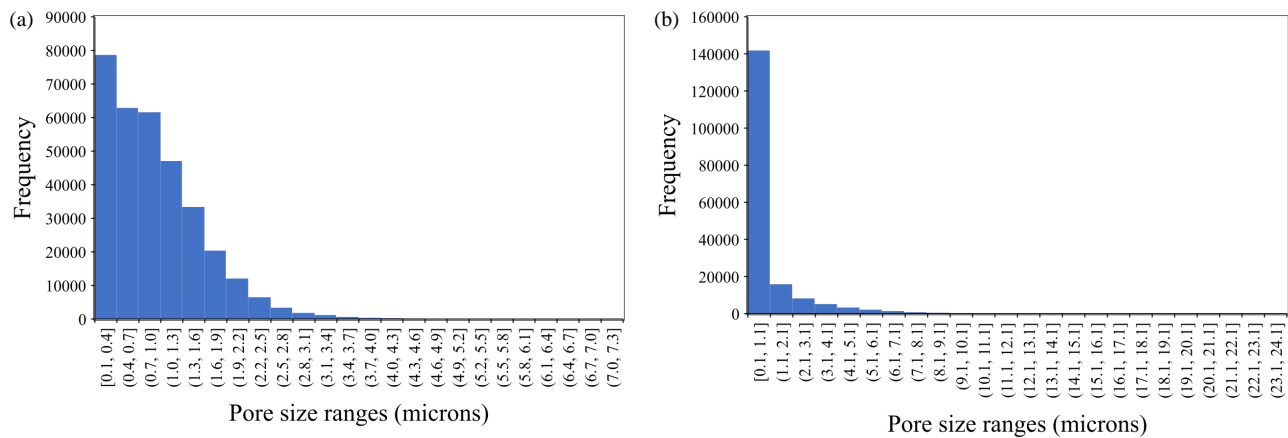


Fig. 3. Pore size distributions of (a) Bentheimer sandstone and (b) Savonnieres carbonate.

Table 1. Properties of micro-CT data.

Parameters	Bentheimer sandstone	Savonnieres carbonate
Image resolution	5.4 microns	3.8 microns
Porosity	24.60%	22.8%
Original size	600^3 voxels	1000^3 voxels

As seen in Figs. 2 and 3, Bentheimer has homogeneous pore size distribution (spreading over a span of 0-7.2 microns) while the Savonnieres carbonate has heterogeneous pore size distribution (spreading over 0-24 microns). This will enable us to examine the robustness of developed models by using samples with two different levels of heterogeneity.

2.5 Meshing

The “OpenFoam” tool “SnappyHexMesh” was used to discretise micro-CT images for simulations (Greenshields, 2022). This tool enables the creation of coarse beginning meshes and 2D and 3D hexahedral meshes from triangulated surface

geometry. These meshes are refined and morphed during many iterative processes to reach this triangulated surface geometry. Having a starting mesh with grid blocks four times larger than the voxels of the initial micro-CT picture is crucial (Fig. 4(a)). Grid blocks of nearby triangulated surface geometry were sliced in half twice at the same time. As a result, the ultimate size of these grid blocks roughly matches the size of a micro-CT voxel (Fig. 4(b)).

The surface of the porous void space can be obtained using the afore-mentioned method, but internal connection is not affected because interpolation for the triangulated surface geometry is not used. In addition, compared to meshes created directly from micro-CT scans, the method can result in a reduction in the number of grid blocks by up to several tens of times as well as an equivalent decrease in calculation time. Additionally, the surface roughness of the walls and the progressive shift in the volumes of adjacent grid blocks can be preserved when automatically refining the thin throats (bottlenecks) of a micro-CT image that comprises of a few voxels.

An additional Python™ script to extract a triangulated

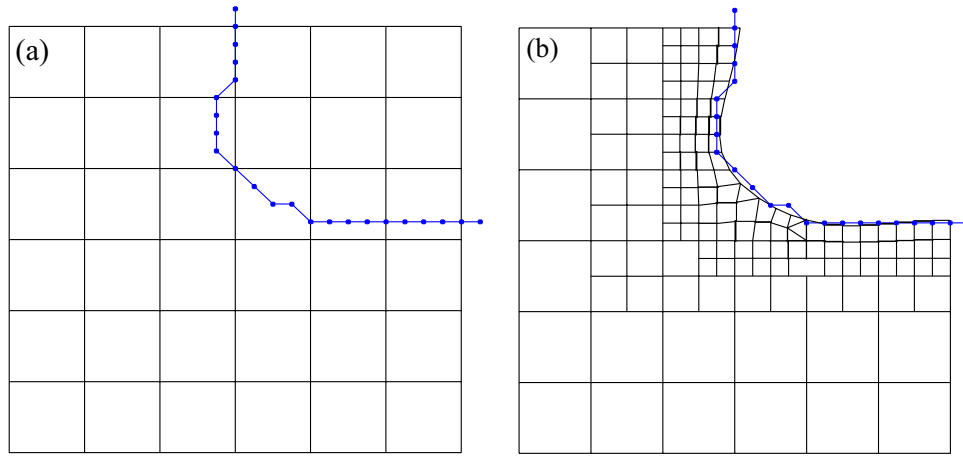


Fig. 4. Conceptual demonstration of meshing technique from (a) starting mesh to (b) final mesh. Black lines represent mesh, while blue lines with nodes represent triangulated surface geometry. Depicted nodes located in neighbouring voxels of micro-CT image.

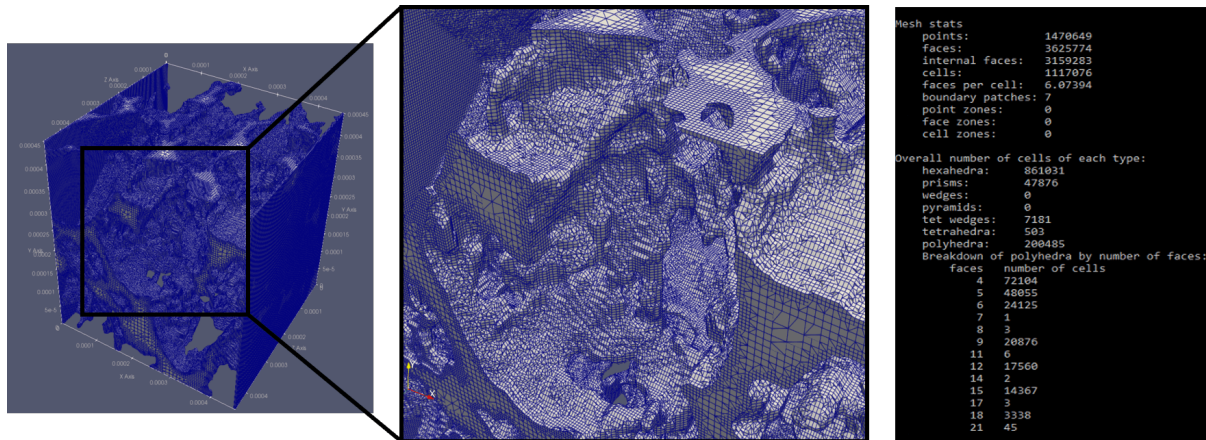


Fig. 5. Generated mesh distributions on 200 cubic voxels sample of Bentheimer sandstone with details of mesh types (right) using CheckMesh utility of OpenFoam.

surface geometry from a segmented micro-CT image was created to implement the meshing technique indicated above. Further, the Python™ script can create extra layers for inlet and outlet boundaries, generate the corresponding original mesh, and compile the results into an “OpenFoam” case using the appropriate templates and extra parameters. Fig. 5 is an example of a final mesh generated over a real rock sample. This approach overcomes the shortcomings of earlier methodologies where single shape grids were used to discretise the pore space, by using a very fine mesh distribution together with variable shapes. Additionally, it makes possible to extract edges and surface features from rock samples with greater accuracy.

2.6 Grid convergence

Mesh resolution has a substantial effect on the outcome of flow simulations by producing discrepancy between results. Grid convergence is therefore required to determine the optimal mesh sizes for a rock sample. This is done to save proce-

Table 2. Transport properties (Hussain et al., 2021).

Phase	Density (kg/m ³)	Kinematic viscosity (m ² /s)	Surface tension (N/m)
Water	1000	1E-06	0.02
Oil	755	1E-06	

ssing time while maintaining the same level of precision as that of a higher resolution mesh. For this purpose, 75 cubic voxels sample of Bentheimer sandstone was utilized with variable mesh enlargement criteria (increased until sample is percolating). Transport properties are summarized in Table 2, and the pressure difference was recorded when the flow was stabilized while maintaining a constant velocity. Absolute permeability was calculated via Darcy’s law, and values were normalized by the absolute permeability of sample with finer mesh. According to the results summarized in Table 3, a mesh enlargement criterion of 8 delivers comparable results to a finer mesh enlargement criterion of 4 for Bentheimer sandstone. Si-

Table 3. Grid convergence data for Bentheimer sandstone (Sample size is 75 cubic voxels).

Mesh enlargement criteria	Absolute permeability (Darcy)	Normalization based on finer mesh
4	1.394	1.00
5	1.342	0.96
6	1.521	1.09
7	1.474	1.06
8	1.391	0.99
9	1.124	0.81
10	0.995	0.71
11	0.837	0.60
12	0.708	0.51

imilarly, mesh enlargement of 7 was found to be the optimum criterion for Savonnières carbonate.

2.7 Model benchmarking

The segmented binary image of Bentheimer sandstone was first extracted to obtain the derivative models of progressively larger sizes. Using custom Python™ scripts and the SnapPyHexMesh dictionary from OpenFoam, the pore space discretization process was carried out after the appropriate mesh enlargement conditions were established using grid convergence. To establish REV using absolute permeability values, single phase simulations were performed. Fig. 6 shows (a) derivative models up to 200 cubic voxels and (b) visualizations of their flow simulations.

Results of single-phase REV calculations by absolute permeability were compared with those of a previously published work to serve as a benchmark (Singh et al., 2020). For the REV estimations of several rocks, including Bentheimer, they used a gray level size zone matrix (GLSZM) technique in conjunction with a finite volume solver. Our work utilizes the same segmented micro-CT data to establish common ground, the only differences are the tools and methods to reach the end result.

The VOF method utilized was based on asymptotic homogenization using constant pressure difference. Our model was set up with constant pressure boundaries, and when a steady state was reached, the final velocity was recorded. Up until REV was established, Darcy law was utilised to estimate the absolute permeability values for increasing sub-volume sizes. The results of the GLSZM with regards to increasing domain size are presented side by side with normalised permeability values in Fig. 7. It should be noted that the GLSZM results serve as a lower bound (underestimation of absolute permeability at smaller sample sizes) while the VOF results serve as an upper bound (overestimation of absolute permeability at smaller sample sizes) which stabilize when REV is achieved. This shows a good agreement between two approaches demonstrating that REV is established at and above

120 cubic voxels (0.7 mm linear length).

2.8 Entropy production

The application of thermodynamic principles requires simplifying assumptions to be able to relate results to the well-established principles of equilibrium thermodynamics. This work utilizes the assumption of thermostatic conditions which allows macroscopic out of equilibrium conditions to be described by connected local equilibrium states where only mass, but no heat is exchanged between the connected local thermal equilibrium states (as shown in Fig. 8).

Entropy is a thermodynamic quantity that depicts the degree of disorder or uncertainty present in a system, which in our case, is the mass flow in and out of the local equilibrium states. In finite volume simulations, the volumes are mainly grid blocks by which the entire domain is discretised. Mass flow for every grid block is solved numerically, the output of which is fed into neighbouring grid blocks as the simulation progresses. Due to their ability to produce their own entropy and contribute to the system's total entropy production, grid blocks can be interpreted as "micro-engines" for multiscale thermodynamic boundary conditions" (Veveakis and Regenauer-Lieb et al., 2015). The rate of entropy production generalizes as the domain increases in size towards the REV because the dissipation by these micro engines averages out, yielding similar petrophysical results. In the thermostatic interpretation the individual "micro-engines" are assumed to operate in a cyclical manner such that within the cycle the heat flow in and out of the volume is reversible and on long time scales the temperature T is constant $\oint dQ_{rev}/T = 0$.

Following Kjelstrup et al. (2018), this work defines a chemical thermodynamic force $d\mu_i^c/dx$ and consider the dissipative work done by the pressure gradient dP/dx on the volume element V_i . Following equation obtains the generalized thermodynamic force $d\mu_{i,T}/dx$ as a potential difference that combines work done over V_i and chemical potential changes inside the REV at constant temperature:

$$\frac{d\mu_{i,T}}{dx} = \frac{d\mu_i^c}{dx} + V_i \frac{dP}{dx} \quad (7)$$

where $d\mu_i^c/dx$ describes the change in chemical potential by changing composition of the medium and if the composition is uniform, this term is neglected. Therefore, differential of chemical potential for a uniform composition in a steady gravitational field is given by:

$$\frac{d\mu_{i,T}}{dx} = -V_i Dg \quad (8)$$

where D is the total mass density and g is the acceleration due to gravity. The associated entropic thermodynamic flux J_s is:

$$J_s = \frac{1}{T} J'_q + \sum_{i=1}^n J_i S_i \quad (9)$$

where J'_q refers to the heat flux and J_i to the mass fluxes. The mass flux is produced by each individual entropy producing volume element at local equilibrium, flowing through a surface of the volume element have units $m^3/(m^2 \cdot s) = m/s$. S_i is th-

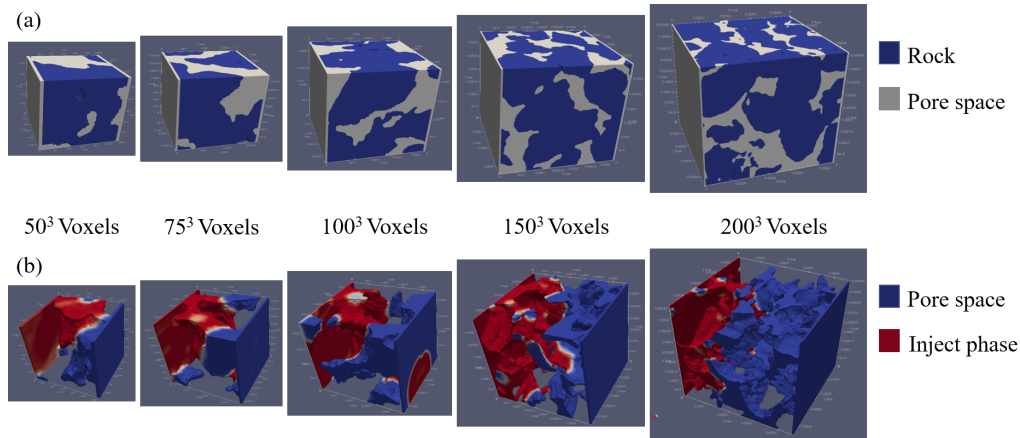


Fig. 6. Illustration of (a) sub-volumes and (b) flow simulations for REV estimation.

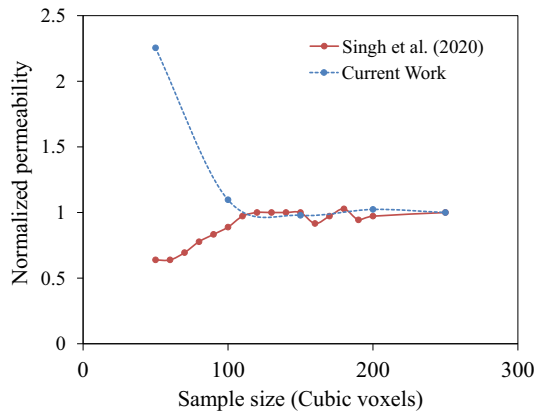


Fig. 7. Normalized absolute permeability results of sub-volumes plotted against similar results from Singh et al. (2020).

e partial entropy production of the internal processes in units $J/(Kg \cdot K)$. Using the Onsager conjugacy assumption of thermodynamic forces and fluxes, a local equilibrium of each thermodynamic engine using the maximum entropy production assumption is obtained. Therefore, the equation for overall entropy production $\partial S/\partial t$ can be written as:

$$\frac{\partial S}{\partial t} = J'_q \frac{\partial}{\partial x} \left(\frac{1}{T} \right) - \frac{1}{T} \sum_{i=1}^n J_i \frac{\partial \mu_{i,T}}{\partial x} \quad (10)$$

In case of two immiscible fluids, component i is distributed into wetting “ w ” and non-wetting “ n ” terms which will modify the above equation as:

$$\frac{\partial S}{\partial t} = J'_q \frac{\partial}{\partial x} \left(\frac{1}{T} \right) - \frac{1}{T} \left(J_w \frac{\partial \mu_{w,T}}{\partial x} + J_n \frac{\partial \mu_{n,T}}{\partial x} \right) \quad (11)$$

Based on the explanations regarding volume flows which were assumed to be Euler homogeneous functions of the first order (Hansen et al., 2018; Kjølstrup et al., 2018), the above equation can be further simplified into:

$$\frac{\partial S}{\partial t} = J'_q \frac{\partial}{\partial x} \left(\frac{1}{T} \right) - \frac{1}{T} \left(v_w \frac{\partial p_w}{\partial x} + v_n \frac{\partial p_n}{\partial x} \right) \quad (12)$$

Since this work focuses on an isothermal system, the first term related to heat transfer is neglected and only the second

term of the equation containing velocities v and pressure gradients $\partial p/\partial x$ of phases, determines overall entropy production. Here the fluid’s specific entropy is dependent on its thermodynamic state, which can be characterized by factors such as pressure, temperature, flow rate and composition. It is to be noted that solid deformation is neglected in the above formulations.

As the aim of above formulations is to calculate mean entropy production in $W/(m^3 \cdot K)$ for each increasing sub-domain, the results can be normalized by their respective volume V making them comparable to each other for REV purposes. This will make our measurements consistent with the ones presented by Niederau et al. (2016) based on hydrothermal models of Central Perth Basin, thereby providing a reference point to compare our results with.

3. Results

The existence and size of an REV in terms of hydrodynamic continuum to describe multiphase flow in reservoir rocks is determined in this work using a variational thermodynamic approach. An asymptotic homogenization technique is employed by considering single and multiphase fluid flows. The expected range for constitutive material parameters in the continuum limit is assessed by alternate Dirichlet and von Neumann boundary conditions. In the thermodynamic approach the former is a constant thermodynamic force (namely, a fixed pressure difference) and the latter a thermodynamic flux (namely, a fixed flow rate on the boundaries). This method has been successfully used as an extension to the variational principle of mechanics for estimation of the extrema of entropy production (minimum and maximum) which upon convergence provide valid bounds of continuum material properties (Regenauer-Lieb et al., 2010, 2013). If convergence is achieved, it results in a thermodynamically consistent REV. For its first application to multiphase porous media flow, this work proposes that it captures the uncertainties introduced by dynamic time-dependent multi-phase flow phenomena such as ganglion flow and local eddies in narrow pore throats. If convergence cannot be achieved for the size of the volume under consideration, it means that the continuum REV assumption

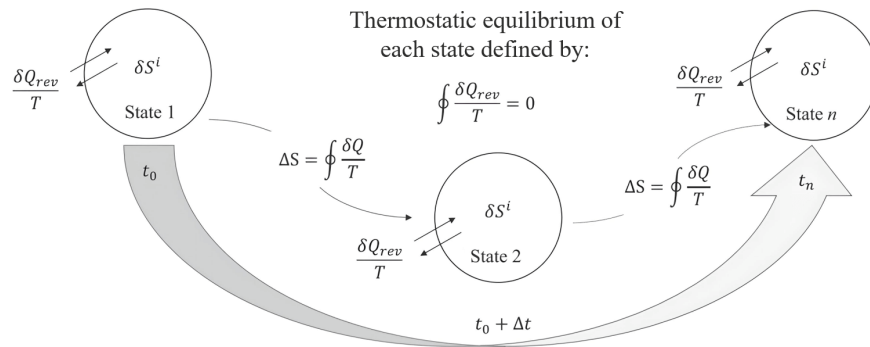


Fig. 8. Thermostatic equilibrium states (Jacquey and Regenauer-Lieb, 2021).

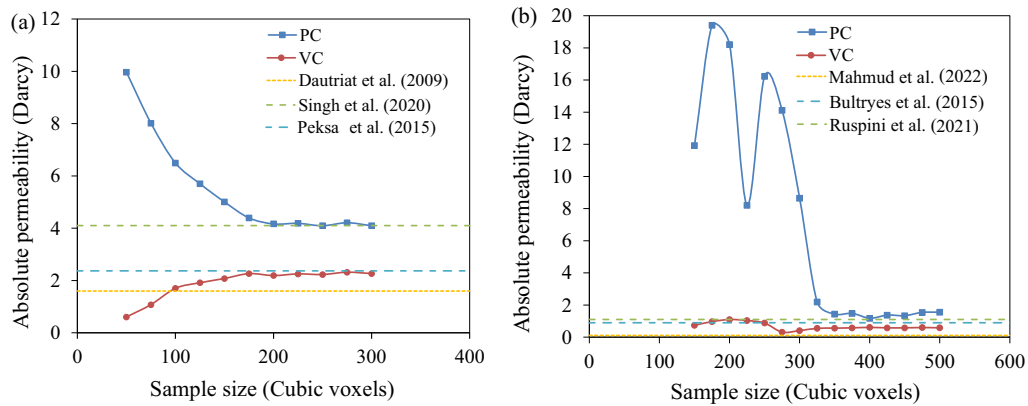


Fig. 9. Asymptotic homogenization of upper and lower hydrodynamic bounds for absolute permeabilities of (a) Bentheimer sandstone and (b) Savonnières carbonate. Dashed lines indicate absolute permeabilities estimated by various authors.

either requires larger reference volumes or that the continuum assumption is not a valid one.

The appropriate thermodynamic REV is found upon convergence of the entropic bounds when an acceptable value of uncertainty is achieved for the postulation of asymptotic homogeneity. The approach is generic and can be applied to derive any constitutive material property by numerical or experimental analyses (Liu et al., 2018b). In this work, the approach of thermodynamic REV has been established and relative permeabilities of multiphase flow and absolute permeabilities for single phase scenarios numerically estimated.

3.1 Single-phase results

3.1.1 Absolute permeability bounds

Absolute permeability bounds were calculated using a 3-D model derived from micro-CT scans (Fig. 2). Numerical simulations were performed using pressure constant (PC) and velocity constant (VC) boundary conditions with water injection. Fig. 9 displays single phase REV measurements for both rocks with the maximum and minimum ranges of absolute permeabilities. For single phase cases, it is found that together with an increase in sample size the absolute permeability for both PC and VC converges within uncertainty limits to a common value, see Fig. 9 (describing the hydro-

dynamic bounds for PC and VC) and Fig. 10 (describing the thermodynamic bounds for PC and VC). Furthermore, absolute permeability values from available literature for Bentheimer sandstone (Dautriat et al., 2009; Peksa et al., 2015; Singh et al., 2020) and Savonnières carbonate (Bultreys et al., 2015; Ruspini et al., 2021; Mahmud et al., 2022) are also presented to validate current REV estimations of both samples.

As can be seen from Fig. 9, the validity of a continuum assumption is documented by the two hydrodynamic bounds. The hydrodynamic REV has converged for sizes above 200 cubic voxels for the Bentheimer sandstone and 350 cubic voxels for the Savonnières carbonate (about 1.04 mm linear length and 1.33 mm linear length, respectively). The ranges of stabilized absolute permeability for Bentheimer sandstone and Savonnières carbonate are found to be 2.2-4.0 Darcy and 0.6-1.5 Darcy, respectively. The above observation demonstrates that the hydrodynamic bounds have captured the average of the two governing factors, namely grain size distributions (heterogeneity) and accessible pore space (porosity). These results also suggest that the higher porosity of homogeneous rock requires smaller sample size to establish REV (as presented in Fig. 9(a)), whereas higher level of heterogeneity results in a greater difference between upper and lower hydrodynamic limits along with a larger sample size for establishing REV (as can be seen in Fig. 9(b)).

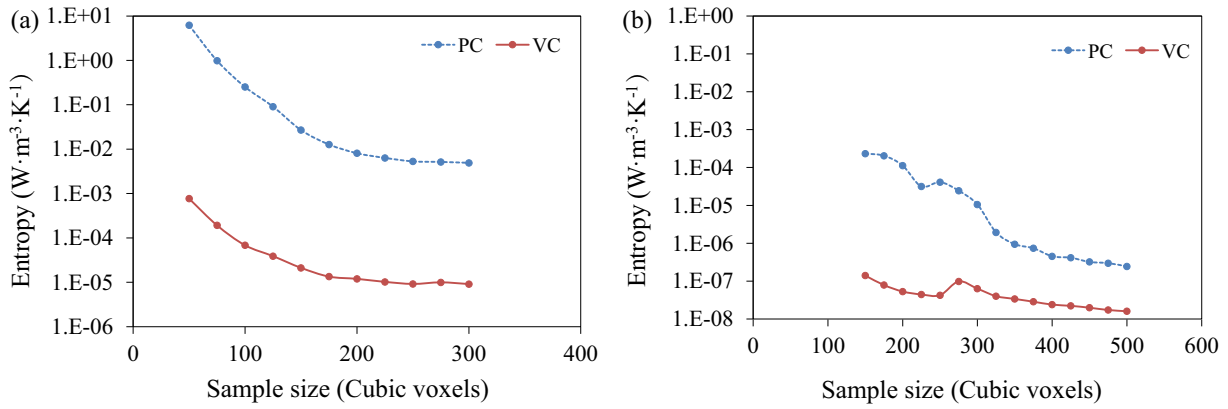


Fig. 10. Single phase upper and lower thermodynamic bounds for entropy production in (a) Bentheimer sandstone and (b) Savonnieres carbonate.

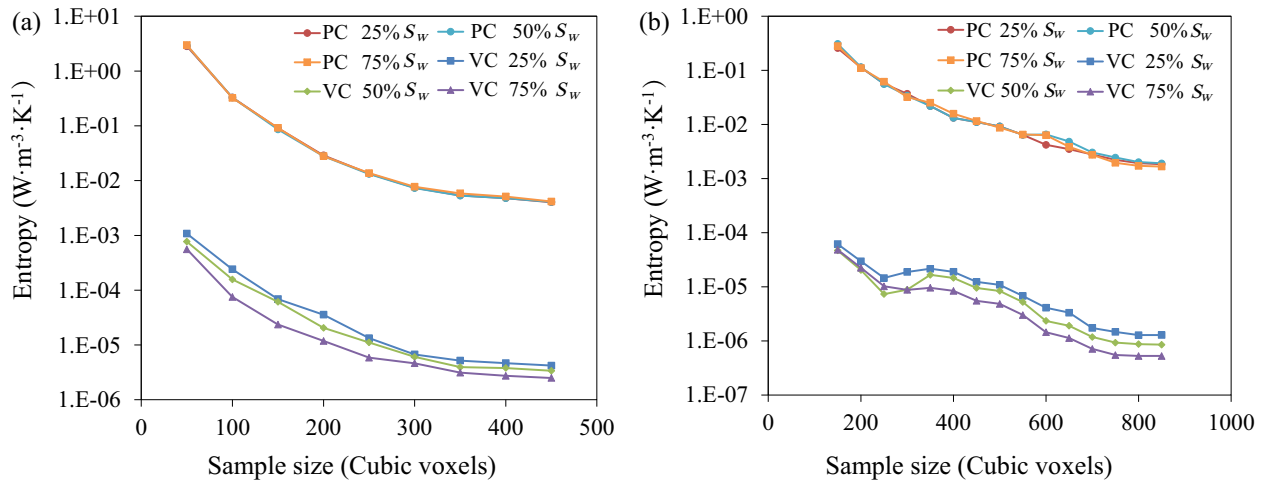


Fig. 11. Multiphase upper and lower thermodynamic bounds for entropy production in (a) Bentheimer sandstone and (b) Savonnieres carbonate.

3.1.2 Entropic bounds

Asymptotic homogenization data based on average rate of entropy production is presented for each sub-volume, which can be utilized to describe how REV is determined for complicated geometrical systems as presented in Fig. 10 for both Bentheimer sandstone and Savonnieres carbonate. In Fig. 10(a), the entropic bounds for Bentheimer sandstone have established an REV at approximately same sample size of 200 cubic voxels, however, the entropic bounds for Savonnieres carbonate (10(b)) have not stabilized as that of the Bentheimer sandstone. An in-depth discussion of this observation is provided in section 4. In terms of boundary conditions, both solutions will eventually converge at REV, however, due to the inherent restrictions in each solution, the results produced by the two methods differ from one another. For instance, due to complex nature of inter-pore connectivity of rocks, a constant pressure solution maintains pressure differential by altering flowrate, which increases turbulence thereby producing highly variable results (see upper bounds in Figs. 9 and 10). This behaviour is expected to be exaggerated when multiple phases

are introduced. The constant flux solution, on the other hand, avoids this problem by preserving the flowrate and subsequently becomes more stable (see lower bounds in Figs. 9 and 10). Therefore, it is preferable to use the constant flux boundary condition to establish REV.

3.2 Multi-phase results

3.2.1 Entropic bounds

For estimating multiphase REV, the same rock configurations and simulation parameters were utilised except for multiple phases (oil 50% and water 50%) being injected concurrently. First, entropic bounds were developed for both the Bentheimer sandstone and the Savonnieres carbonate samples to determine the amount of complexity present in both domains when multiphase flow is considered. Thermodynamic entropic bounds (average entropy production versus sample size) were obtained in Fig. 11 for both pressure and flux boundary conditions to capture the maximum and minimum values of entropy production in all samples. Results

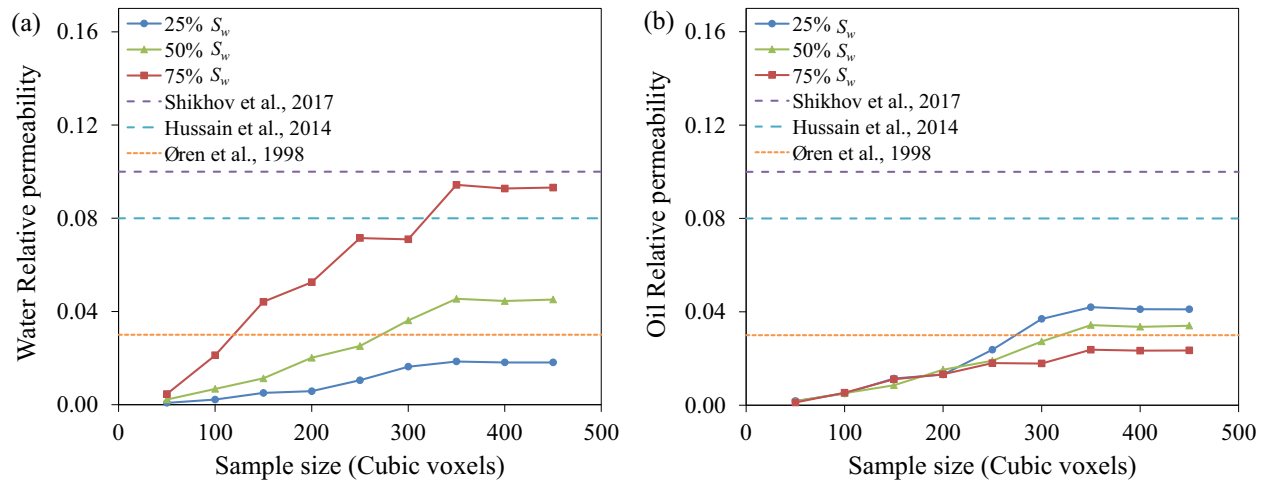


Fig. 12. Constant flux hydrodynamic bounds for relative permeabilities of (a) water and (b) oil in Bentheimer sandstone.

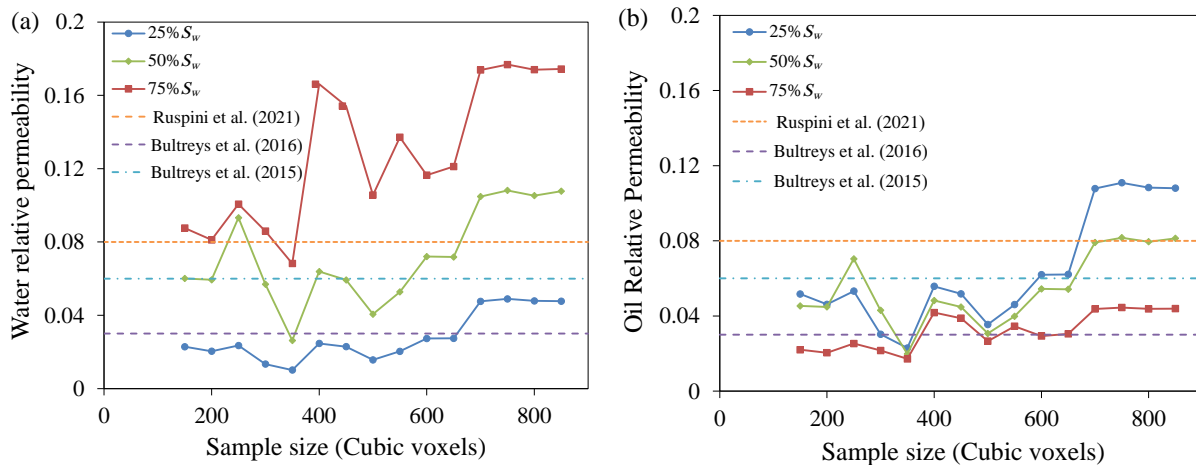


Fig. 13. Constant flux hydrodynamic bounds for relative permeabilities of (a) water and (b) oil in Savonnieres carbonate.

demonstrate a significant difference between the two boundary conditions with an overall decrease in entropy production as the domain size move towards REV.

In Fig. 11, there is a notable difference between the VC bounds of the two rocks, illustrating that the sample with a greater water saturation has lower values of entropy production throughout compared to its counterparts. Due to these variations in entropic values, REV estimates of single-phase differ from multi-phase. For single phase, entropic bounds have established REV estimates above 200 and 350 cubic voxels for Bentheimer sandstone and Savonnieres carbonate, respectively, but for multiphase situations, these REV sample sizes have been increased to 400 and 800 cubic voxels, respectively.

As for multiphase PC entropic bounds, there is no distinction among findings derived at various saturation values (see Figs. 11(a) and 11(b)). Almost all scenarios establish REV estimates at the same sample sizes, which are greater than 400 cubic voxels for Bentheimer sandstone and 800 cubic voxels for Savonnieres carbonate. This implies that the PC bound solely considers geometrical elements of domains when determining

REV and does not properly capture the effects of change in saturations, hence avoiding the complications emerging from multiple phase flow.

3.2.2 Relative permeability bounds

Since the flow rate of a constant pressure boundary condition (upper bound) varies throughout the sample (which increases the turbulence/capillary number in individual phases), only a constant flux boundary condition (lower bound) is utilised to estimate relative permeability (K_r) values for determining REV.

Based on asymptotic homogeneity of VC hydrodynamic bounds, Figs. 12-15 depict multiphase REV estimates for both rock configurations. Water relative permeability (K_{rw}) increases with increasing water saturation (S_w) in all cases (Figs. 12(a) and 13(a)), whereas oil relative permeability (K_{ro}) decreases (Figs. 12(b) and 13(b)). This is because the initial rock conditions are purely water-wet, causing K_{ro} to be greater than K_{rw} at lower S_w values, and as S_w increases, the system provides greater mobility to the water phase. This behaviour

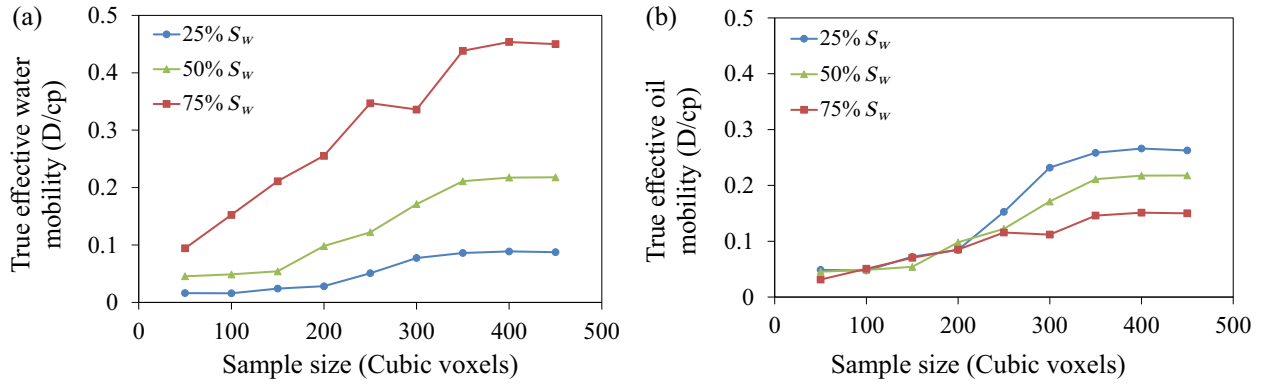


Fig. 14. Constant flux hydrodynamic bounds for TEM of (a) water and (b) oil in Bentheimer sandstone.

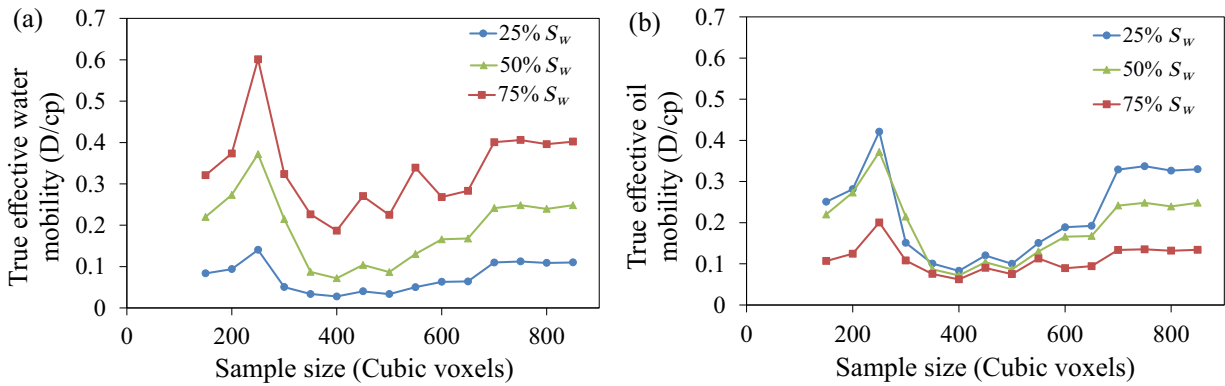


Fig. 15. Constant flux hydrodynamic bounds for TEM of (a) water and (b) oil Savonnieres carbonate.

is typical of a traditional relative permeability curve for a water-wet system. Regarding REV, Figs. 12(a) and 12(b) for Bentheimer sandstone give solid evidence of increased REV above 350 cubic voxels, which is nearly double that of single-phase REV at 200 cubic voxels. These results are consistent with a previous study on a homogeneous sand pack by Liu and Wang (2022). Similarly, Figs. 13(a) and 13(b) show establishment of multi-phase REV for Savonnieres carbonate above 700 cubic voxels, which is double that of single-phase REV at 350 cubic voxels. Furthermore, the multiphase results are validated by employing equal K_r points extracted from K_r curves presented in various studies on Bentheimer sandstone (Øren et al., 1998; Hussain et al., 2014; Shikhov et al., 2017) and Savonnieres carbonate (Bultreys et al., 2015; Bultreys, 2016; Ruspini et al., 2021). Since the simulations for multiphase REV estimations were performed under conditions of constant flux of water and oil at constant initial saturations, it is essential to avoid confusion by refraining from presenting the complete K_r curves for validation. Instead, equal relative permeability points are utilized as a critical representation of the K_r curves and serve the purpose of validation.

3.2.3 True effective mobility bounds

In addition to relative permeability estimation, the True Effect Mobility functions (TEM) are considered as an efficient method for analysing the dynamic characteristics of fluid flow

in porous media combining porosity, permeability, and fluid viscosity (Mirzaei-Paiaman et al., 2019):

$$TEM_{\alpha} = \frac{kk_{r\alpha}}{\phi\mu_{\alpha}} \quad (13)$$

where TEM_{α} is true effective mobility of a phase, k is absolute permeability, $k_{r\alpha}$ is relative permeability of a phase, ϕ is porosity and μ_{α} is the phase viscosity.

TEM bounds for oil and water in Bentheimer sandstone (see Fig. 14) and Savonnieres carbonate (see Fig. 15) exhibited similar behaviour as of VC K_{rw} and K_{ro} hydrodynamic bounds, with the exception of non-overlapping behaviour of bounds (steady and distinct rise) in Savonnieres carbonate configuration.

4. Discussion

An REV is the smallest volume of a porous material representative of its macroscopic properties for single-phase or multiphase fluid systems. The distribution and interactions of distinct fluid phases in a porous medium can have a considerable impact on the flow and transport parameters, influencing REV calculations as well. When describing the macroscopic features of a porous material, particularly in the oil and gas industry, it is crucial to account for the multiphase behaviour. In this regard, the first study on REV evaluation in multiphase fluid flow was proposed by Liu and Wang (2022).

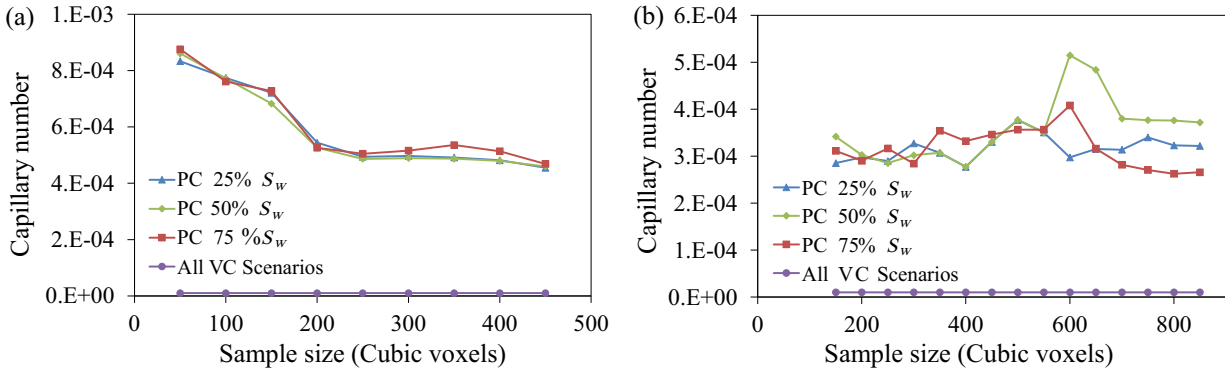


Fig. 16. Capillary numbers during multiphase REV estimations of (a) Bentheimer sandstone and (b) Savonnieres carbonate.

Using an unconsolidated spherical grains pack, the authors determined that the REV of a multiphase porous system is higher than that of a single-phase system. Our study extends this technique to real rock configurations by incorporating the thermodynamic description of maximum and minimum entropic bounds required to comprehend the intricacies of multiphase interactions in porous media. In addition, Liu and Wang (2022) employed the FE-LBM method for numerical simulations, which has its own limitations, particularly when it comes to managing multiphase complexities. Hence, this study employs the VOF approach, a robust and powerful numerical tool that is particularly suitable for simulating complex fluid flow processes and has the following advantages over LBM:

- 1) It offers greater precision than the LBM for modelling complicated fluid flow phenomena, such as free surface flows, multiphase flows, and turbulence.
- 2) The method is more suited than the LBM for simulating a wider variety of fluid flow issues, such as those with high Reynolds numbers, high density and viscosity contrasts, compressibility effects, and massive deformations.
- 3) The VOF method depends less on grid resolution than the LBM. This means that valid findings can be obtained using coarser grids, which can greatly lower processing costs.
- 4) The technique needs less detailed boundary conditions than the LBM. This makes it easier to apply and the method is less susceptible to errors caused by an unsuitable choice of boundary conditions.

For REV estimations based on absolute permeability in Fig. 9, it is found that heterogeneity has a significant impact on the sample size required for REV. This behaviour is also evident in the average entropy production bounds presented in Figs. 10 and 11, the relative permeability bounds in Figs. 12 and 13, and the TEM bounds in Figs. 14 and 15, where a larger sample size is required to determine REV for a rock with heterogeneous pore size distribution (Savonnieres carbonate). Yet, each of the preceding figures has more detailed information describing the behaviour of hydrodynamic and thermodynamic bounds in relation to their rock configurations. For example, all the entropic bounds in Figs. 10 and 11 indicate high values of normalized entropy production when

the sample size is small, which greatly reduce and stabilize as the system move towards REV because the entropy produced by micro-engines (grid blocks) becomes constant. Noting that the entropic bounds are represented on a logarithmic scale, the difference between the upper and lower bounds at smaller sizes is very large in comparison to REV, indicating convergence of both bounds. Furthermore, the entropic bounds obtained from the PC boundary condition for multiphase in Figs. 11(a) and 11(b) are incapable of capturing the effects of different fluid saturations, hence avoiding the difficulties originating from multiphase flow. This is the result of uncontrolled capillary numbers in PC situations, which is a dimensionless measure of the relative effect of viscous forces and surface tension at the interface of two fluids. When the capillary number exceeds a specific value (10^{-5}), viscous forces dominate and the interface between phases is disturbed, leading in significant multiphase complexity such as snap-off, ganglion flow, development of new channels, and rapid pressure rise, among others. The following equation is used to estimate the dimensionless capillary number (N_c), and the only modifiable parameter in our models is the velocity (v in m/s) of the injected phase, since water viscosity (μ_w in Pa·s) and oil/water interfacial tension (σ_{ow} in N/m) were held constant throughout. Therefore, PC boundary condition is unable to maintain constant flux/velocity, leading in a fluctuating capillary number (see Fig. 16) and an indistinguishable response of PC bounds:

$$N_c = \frac{\mu_w v}{\sigma_{ow}} \quad (14)$$

Both hydrodynamic and thermodynamic approaches are utilised in this paper to demonstrate the existence of an REV. For single-phase, the hydrodynamic approach as well as the thermodynamic approach found the REV of Bentheimer sandstone above 200 cubic voxels in Figs. 9(a) and 10(a). Similarly, the hydrodynamic bounds for Savonnieres carbonate indicated REV values above 350 cubic voxels in Fig. 9(b), whereas thermodynamic bounds produce very close values above 375 cubic voxels, however, the bounds do not stabilize (see Fig. 10(b)). This is due to the higher level of heterogeneity present in carbonate rocks resulting in irregular dissipation by the micro engines even when the hydrodynamic bounds have stabilized. These observations demonstrate that Bentheimer

sandstone and Savonnieres carbonate establish single-phase REV at volumes greater than 200 and 375 cubic voxels, respectively.

To prevent producing additional data and save computational time, relative permeability and TEM bounds are only generated for the VC boundary condition based on the preceding information. As for multiphase, the hydrodynamic approach found the REV of Bentheimer sandstone to be above 350 cubic voxels (see Figs. 12 and 14), whereas thermodynamic REV is established above 400 cubic voxels (see Fig. 11(a)). On the other hand, REV for Savonnieres carbonate is established above 700 cubic voxels by hydrodynamic bounds (see Figs. 13 and 15) and above 800 cubic voxels by thermodynamic bounds (see Fig. 11(b)). These findings demonstrate that Bentheimer sandstone and Savonnieres carbonate establish multiphase REV at volumes greater than 400 and 800 cubic voxels. Therefore, it can be concluded that the REV of a typical sandstone rock is twice that of a single-phase estimate, whereas, for a typical carbonate rock, it is more than twice. This has been determined after analysing findings for various wetting saturations, even though inherent variances exist among the results.

The VC hydrodynamic bounds of relative permeabilities for Bentheimer sandstone (see Fig. 12) indicate a continuous rise and unique behaviour until the REV is reached, however, the Savonnieres carbonate configuration (see Fig. 13) displays random behaviour prior to REV. Given the fact that Savonnieres carbonate is comprised of non-uniform particle shapes and sizes, these behaviour patterns indicate that pore size distribution is the primary cause. However, TEM bounds for Savonnieres carbonate (see Fig. 15) show a steady increase in bounds which indicates that TEM function is a significantly more accurate depiction of the dynamic quality of rock, producing stable results even for systems with comparatively heterogeneous pore size distributions. In addition, K_{ro} bounds (Figs. 12(b) and 13(b)) and TEM-oil bounds (Figs. 14(b) and 15(b)) prior to REV, exhibit overlapping results, like what was found for multiphase PC entropic bounds (Figs. 11(a) and 11(b)). This suggests that dynamic heterogeneity resulting from non-wetting phase complexity is accountable for these observations. In contrast, K_{rw} bounds (Figs. 12(a) and 13(a)) and TEM-water bounds (Figs. 14(a) and 15(a)) exhibit a distinct depiction of each bound with a constant increase up until REV.

5. Conclusions

This study examines the asymptotic hydrodynamic homogenization process for determining the REV of porous media and the key distinctions between single and multiphase estimates. To further corroborate the data, thermodynamic bounds for the average rate of entropy production as well as the hydrodynamic properties of rocks, such as TEM, relative permeabilities, and absolute permeability, were added. This is accomplished by performing finite volume simulations utilizing the open-source platform called OpenFoam and a customized variable mesh generation algorithm to optimize the discretization of pore space. Following are main outcomes

of this research:

- 1) Thermodynamic bounds offer a clearer understanding of how the energy dissipation is influenced by the dynamic rock qualities. Hydrodynamic bounds, on the other hand, capture the dynamics of flow behaviour in porous media.
- 2) For single phase, increasing degrees of heterogeneity lead to a wider discrepancy between upper and lower bounds and requires a larger sample size to establish REV. Whereas, for multiphase, due to uncontrolled flowrates which increases phase complexity, constant pressure estimates are extremely complicated and generate indistinguishable results. Therefore, only constant flux estimates are suitable for generating relative permeability values because they maintain controlled capillary numbers.
- 3) For entropy generation in VC bounds, the rate of entropy production decreases as the wetting phase saturation rises because the work performed by micro engines becomes constant, stabilizing the rate of entropy formation as the domain size move towards REV.
- 4) When compared to single-phase estimates, the multiphase REV for Bentheimer sandstone requires twice the sample size whereas it is more than twice for Savonnieres carbonate.
- 5) The TEM function is a useful tool for illustrating the dynamic quality of rocks, which yields steady and distinguishable findings even in heterogeneous settings.

In summary, a significant contribution has been made to our current knowledge by developing a robust method for evaluating REV in multiphase flow dynamics problems. However, it is important to note that this study is only a pilot study aimed at investigating the effects of multiple phases on REV estimations of actual rock samples. Further work and improvements are required to gain a deeper understanding of this area.

In particular, the multiscale approach plays a crucial role in addressing the numerous micrometre to millimetre scale heterogeneities inherent in carbonate rocks. This approach necessitates the use of specialized mesh generation algorithms to accurately account for multiple scales. Additionally, a specifically tailored numerical solver is required to effectively handle multiple phases and the complexities of their interfaces in all regions. Expanding this research to a multiscale level would require a significantly larger sample size than what was utilized in this study, as well as substantial computational resources. Furthermore, this work does not document the effects of partial entropies, changes in fluid saturations, and wettability alteration on REV estimation. Exploring these factors represents an unexplored area of research that merits further investigation.

Acknowledgements

Shaheryar T. Hussain would like to acknowledge the support from Australian Government and University of New South Wales for providing RTP scholarship of his PhD.

Conflict of interest

The authors declare no competing interest.

Open Access This article is distributed under the terms and conditions of the Creative Commons Attribution (CC BY-NC-ND) license, which permits unrestricted use, distribution, and reproduction in any medium, provided the original work is properly cited.

References

- Aliseda, A., Heindel, T. J. X-ray flow visualization in multi-phase flows. *Annual Review of Fluid Mechanics*, 2021, 53: 543-567.
- Alpak, F. O., Berg, S., Zacharoudiou, I. Prediction of fluid topology and relative permeability in imbibition in sandstone rock by direct numerical simulation. *Advances in Water Resources*, 2018, 122: 49-59.
- Al-Raoush, R., Papadopoulos, A. Representative elementary volume analysis of porous media using X-ray computed tomography. *Powder Technology*, 2010, 200(1-2): 69-77.
- Aniszewski, W., Ménard, T., Marek, M. Volume of fluid (VOF) type advection methods in two-phase flow: A comparative study. *Computers & Fluids*, 2014, 152: 193-194.
- Bear, J. Dynamics of fluids in porous media. *Soil Science*, 1975, 120: 162-163.
- Bultreys, T., Stappen, J. V., Kock, T. D., et al. Investigating the relative permeability behavior of microporosity-rich carbonates and tight sandstones with multiscale pore network models. *Journal of Geophysical Research: Solid Earth*, 2016, 121(11): 7929-7945.
- Bultreys, T., Van Hoorebeke, L., Cnudde, V. Multi-scale, micro-computed tomography-based pore network models to simulate drainage in heterogeneous rocks. *Advances in Water Resources*, 2015, 78: 36-49.
- Costanza-Robinson, M. S., Estabrook, B. D., Fouhey, D. F. Representative elementary volume estimation for porosity, moisture saturation, and air-water interfacial areas in unsaturated porous media: Data quality implications. *Water Resources Research*, 2011, 47(7): W07513.
- Dai, Z., Middleton, R., Viswanathan, H., et al. An integrated framework for optimizing CO₂ sequestration and enhanced oil recovery. *Environmental Science & Technology Letters*, 2014, 1(1): 49-54.
- Dautriat, J., Gland, N., Guelard, J., et al. Axial and radial permeability evolutions of compressed sandstones: End effects and shear-band induced permeability anisotropy. *Pure and Applied Geophysics*, 2009, 166(5): 1037-1061.
- Deshpande, S. S., Anumolu, L., Trujillo, M. F. Evaluating the performance of the two-phase flow solver interFoam. *Computational Science & Discovery*, 2012, 5(1): 014016.
- Diwakar, M., Kumar, M. A review on CT image noise and its denoising. *Biomedical Signal Processing and Control*, 2018, 42(1): 73-88.
- Dong, H., Blunt, M. J. Pore-network extraction from micro-computerized-tomography images. *Physical Review E*, 2009, 80(3): 036307.
- Gharbi, O., Blunt, M. J. The impact of wettability and connectivity on relative permeability in carbonates: A pore network modeling analysis. *Water Resources Research*, 2012, 48(12): W12513.
- Greenshields, C. *OpenFOAM v10 User Guide*, 2022.
- Hansen, A., Sinha, S., Bedeaux, D., et al. Relations between seepage velocities in immiscible, incompressible two-phase flow in porous media. *Transport in Porous Media*, 2018, 125(3): 565-587.
- Hirt, C. W., Nichols, B. D. Volume of fluid (VOF) method for the dynamics of free boundaries. *Journal of Computational Physics*, 1981, 39(1): 201-225.
- Hussain, F., Pinczewski, W. V., Cinar, Y., et al. Computation of relative permeability from imaged fluid distributions at the pore scale. *Transport in Porous Media*, 2014, 104(1): 91-107.
- Hussain, S. T., Rahman, S. S., Azim, R. A., et al. Multiphase fluid flow through fractured porous media supported by innovative laboratory and numerical methods for estimating relative permeability. *Energy & Fuels*, 2021, 35(21): 17372-17388.
- Jacquey, A. B., Regenauer-Lieb, K. Thermomechanics for geological, civil engineering and geodynamic applications: Rate-dependent critical state line models. *Rock Mechanics and Rock Engineering*, 2021, 54(10): 5355-5373.
- Jiang, F., Tsuji, T. Estimation of three-phase relative permeability by simulating fluid dynamics directly on rock-microstructure images. *Water Resources Research*, 2017, 53(1): 11-32.
- Joekar-Niasar, V., van Dijke, M. I. J., Hassanizadeh, S. M. Pore-scale modeling of multiphase flow and transport: Achievements and perspectives. *Transport in Porous Media*, 2012, 94(2): 461-464.
- Karnakov, P., Litvinov, S., Koumoutsakos, P. A hybrid particle volume-of-fluid method for curvature estimation in multiphase flows. *International Journal of Multiphase Flow*, 2020, 125: 103209.
- Khodadadi, B., Qadeer Siddiqui, M. A., Pirzada, M. A., et al. Direct observation of two-phase flow in deformable fractures of shales: A Utica shale example. *Journal of Petroleum Science and Engineering*, 2020, 194: 107487.
- Kjelstrup, S., Bedeaux, D., Hansen, A., et al. Non-isothermal transport of multi-phase fluids in porous media. The entropy production. *Frontiers in Physics*, 2018, 6: 126.
- Lanetc, Z., Zhuravljov, A., Armstrong, R. T., et al. Hybrid numerical methods for modelling multi-physics mass transport in coal. *International Journal of Heat and Mass Transfer*, 2023, 214: 124386.
- Leu, L., Berg, S., Enzmann, F., et al. Fast X-ray micro-tomography of multiphase flow in berea Ssandstone: A sensitivity study on image processing. *Transport in Porous Media*, 2014, 105: 451-469.
- Liao, Q., Xue, L., Wang, B., et al. A new upscaling method for microscopic fluid flow based on digital rocks. *Advances in Geo-Energy Research*, 2022, 6(4): 357-358.
- Liu, T., Jin, X., Wang, M. Critical resolution and sample size of digital rock analysis for unconventional reservoirs. *Energies*, 2018a, 11: 1798.
- Liu, J., Regenauer-Lieb, K. Application of percolation theory

- to microtomography of rocks. *Earth-Science Reviews*, 2021, 214: 103519.
- Liu, J., Sarout, J., Zhang, M., et al. Computational upscaling of Drucker-Prager plasticity from micro-CT images of synthetic porous rock. *Geophysical Journal International*, 2018b, 212: 151-163.
- Liu, T., Wang, M. Critical REV size of multiphase flow in porous media for upscaling by pore-scale modeling. *Transport in Porous Media*, 2022, 144(1): 111-132.
- Liu, T., Zhang, S., Wang, M. Does rheology of bingham fluid influence upscaling of flow through tight porous media? *Energies*, 2021, 14(3): 680.
- Mahmud, H. B., Khalifa, M., Shafiq, M., et al. Experimental investigation of the influence of carbonated water on sandstone and carbonate rock properties. *Petroleum Research*, 2022, in press, <https://doi.org/10.1016/j.ptlrs.2022.10.007>.
- Mirzaei-Paiaman, A., Saboorian-Jooybari, H., Chen, Z., et al. New technique of true Effective mobility (TEM-Function) in dynamic rock typing: Reduction of uncertainties in relative permeability data for reservoir simulation. *Journal of Petroleum Science and Engineering*, 2019, 179: 210-227.
- Mostaghimi, P., Blunt, M. J., Bijeljic, B. Computations of absolute permeability on micro-CT images. *Mathematical Geosciences*, 2013, 45(1): 103-125.
- Moukalled, F., Mangani, L., Darwish, M. *The Finite Volume Method in Computational Fluid Dynamics: An Advanced Introduction with OpenFOAM® and Matlab*. New York, USA, Springer International Publishing, 2016.
- Niederer, J., Clauser, C., Börsing, N., et al. Entropy production and attractors: Measures to quantify uncertainty and complexity introduced by convection. Paper Presented at the European Geothermal Conference, Strasbourg, France, 19-24 September, 2016.
- Øren, P. E., Bakke, S., Arntzen, O. J. Extending predictive capabilities to network models. *SPE Journal*, 1998, 3(4): 324-336.
- Patankar, S. *Numerical Heat Transfer and Fluid Flow*. Boca Raton, USA, CRC Press, 2018.
- Pavuluri, S., Maes, J., Doster, F. Spontaneous imbibition in a microchannel: Analytical solution and assessment of volume of fluid formulations. *Microfluidics and Nanofluidics*, 2018, 22(8): 90.
- Peksa, A. E., Wolf, K. H. A. A., Zitha, P. L. J. Bentheimer sandstone revisited for experimental purposes. *Marine and Petroleum Geology*, 2015, 67: 701-719.
- Pirzada, M. A., Bahaaddini, M., Andersen, M. S., et al. Coupled hydro-mechanical behaviour of rock joints during normal and shear Loading. *Rock Mechanics and Rock Engineering*, 2023, 56: 1219-1237.
- Ramstad, T., Berg, C. F., Thompson, K. Pore-scale simulations of single- and two-phase flow in porous media: Approaches and applications. *Transport in Porous Media*, 2019, 130(1): 77-104.
- Regenauer-Lieb, K., Hu, M., Schrank, C., et al. Cross-diffusion waves resulting from multiscale, multiphysics instabilities: Application to earthquakes. *Solid Earth*, 2021a, 12: 1829-1849.
- Regenauer-Lieb, K., Hu, M., Schrank, C., et al. Cross-diffusion waves resulting from multiscale, multi-physics instabilities: Theory. *Solid Earth*, 2021b, 12(8): 869-883.
- Regenauer-Lieb, K., Karrech, A., Chua, H. T., et al. Time-dependent, irreversible entropy production and geodynamics. *Philosophical Transactions of the Royal Society A: Mathematical, Physical and Engineering Sciences*, 2010, 368(1910): 285-300.
- Regenauer-Lieb, K., Karrech, A., Chua, H., et al. Entropic bounds for multi-scale and multi-physics coupling in earth sciences. *Beyond the Second Law*, 2014: 323-335.
- Regenauer-Lieb, K., Veveakis, M., Poulet, T., et al. Multiscale coupling and multiphysics approaches in earth sciences: Theory. *Journal of Coupled Systems and Multiscale Dynamics*, 2013, 1(1): 49-73.
- Rusche, H. *Computational Fluid Dynamics of Dispersed Two-Phase Flows at High Phase Fractions*. London, UK, Imperial College London, 2003.
- Ruspini, L. C., Øren, P. E., Berg, S., et al. Multiscale digital rock analysis for complex rocks. *Transport in Porous Media*, 2021, 139(2): 301-325.
- Shapoval, A., Zhuravljov, A., Lanetc, Z., et al. Pore-scale evaluation of physicochemical interactions by engineered water injections. *Transport in Porous Media*, 2023, 148(3): 605-625.
- Shikhov, I., d'Eurydice, M. N., Arns, J. Y., et al. An experimental and numerical study of relative permeability estimates using spatially resolved NMR. *Transport in Porous Media*, 2017, 118: 225-250.
- Sidorenko, M., Orlov, D., Ebadi, M., et al. Deep learning in denoising of micro-computed tomography images of rock samples. *Computers & Geosciences*, 2021, 151: 104716.
- Singh, A., Regenauer-Lieb, K., Walsh, S. D. C., et al. On representative elementary volumes of grayscale micro-CT images of porous media. *Geophysical Research Letters*, 2020, 47(15): e2020GL088594.
- Urakov, D. S., Rahman, S. S., Tyson, S., et al. Conceptualizing a dual porosity occurrence in sandstones by utilizing various laboratory methods. *SOCAR Proceedings*, 2021, 2: 6-16.
- Veveakis, E., Regenauer-Lieb, K. Review of extremum postulates. *Current Opinion in Chemical Engineering*, 2015, 7: 40-46.